Parametric Model Order Reduction of a Thermoelectric Generator for Electrically Active Implants

Cheng Dong Yuan[1,2], Onkar Sandip Jadhav[2], Evgenii B. Rudnyi[3], Dennis Hohlfeld[2], Tamara Bechtold[1,2]
[1]Department of Engineering, Jade University of Applied Sciences, Wilhelmshaven, Germany
[2]Institute for Electronic Appliances and Circuits, University of Rostock, Rostock, Germany
[3] CADFEM GmbH, Munich, Germany
Email: tamara.bechtold@jade-hs.de

Abstract

Thermoelectric generators are investigated as supplementary power sources for electrically active implants. We analyze a thermal model of human tissue with an implanted generator. The impact of convection at the skin surface is studied by applying parametric model order reduction with film coefficient and ambient temperature as parameters. We propose to use our approach for efficient parameter studies and the co-simulation of generator and electric circuitry.

1. Introduction

According to [1], by 2060 one out of three persons in Germany will be over 65 years old. Medical technology, which improves the efficiency of necessary medical treatments, is therefore gaining more concern. The need for developing implantable medical devices for regeneration of bone and cartilage, deep brain simulation or cardiac pacing is rapidly increasing. As those devices are battery-powered, surgery is required to replace the drained energy storage. The related risk and cost of repeated surgery imposes a considerable drawback. We therefore propose to develop self-powered medical implants, which tap into the energy available from the human body itself.

Energy-harvesting technology has shown to bear the potential to increase the operational time of implantable devices [2]–[5]. By harvesting mechanical and thermal energy around or inside the human body, electrical power can be supplied to medical devices. This is achieved by micro-structured piezoelectric or thermoelectric energy generators (TEG) [6], [7].

Implanted TEGs utilize the Seebeck effect to harvest on temperature gradients inside the human body in order to provide electrical power for electrically active implants [8]–[10]. The amount of power delivered, depends on temperature gradients inside the human body. Heat losses by convection, radiation, evaporation (sweating) and conduction determine the heat exchange between the human body and its environment [11]. In this work, we consider only convection at the skin surface and evaluate the impact of the film coefficient and the ambient temperature on the temperature gradient.

To design and optimize such devices, numerical simulation is employed, as it saves fabrication cost and supports device optimization. Using the finite element method (FEM) the governing partial differential equation (PDE) is spatially discretized, resulting in a system of ordinary differential equations (ODEs). The large dimension of such a numerical model leads to high computational costs for transient simulations. Furthermore, parameter studies multiply the computational effort for the static simulation as well.

Mathematical model order reduction (MOR) generates highly accurate and compact reduced order models [12]–[14]. This technique has already been successfully applied to linear thermal models of various microsystems and has proven its robustness [15]. Parametric model order reduction (pMOR) by multi-variate moment-matching as suggested in [16]–[20] is able to provide parametrized reduced order models. This has been successfully demonstrated for various micromachined case studies [21].

In this work, we apply the pMOR methodology for efficient parameter studies, that is to determine how the environmental conditions influence the temperature distribution across the human TEG.

In Section 2 we present the model of the TEG surrounded by human tissue. In Section 3, we describe the parametric MOR process for generating a compact model, which contains the film coefficient and the ambient temperature as parameters. In Section 4 the accuracy of the parameterized reduced order model is verified and its applicability for parameter studies is demonstrated. The impact of heat convection at the skin surface on the temperature difference across the TEG is investigated. Finally, a co-simulation setup of the compact TEG model together with an electronic circuit is presented. Section 5 summarizes this work and gives an outlook to further research.

2. Case Study: Human TEG Model

In this section, a model of a miniaturized thermoelectric generator surrounded by human tissue is presented. Figure 1 illustrates the envisioned electrically active implant consisting of a TEG, energy buffer and application-specific integrated circuit (ASIC). The implant is positioned in the fat layer, in which the maximum temperature gradient has been calculated [22].

The TEG (see Figure 2) consists of two metallic discs (diameter 13 mm, height 0.9 mm) and an array of 9×9 thermocouple legs in between ($\kappa_{th} = 1,35$ W/m/K, $\alpha =$

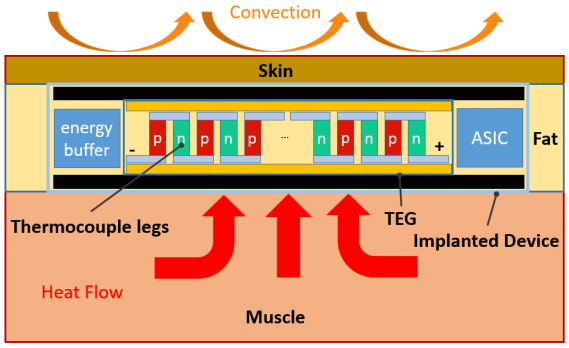

Figure 1: Schematic of a subcutaneous TEG-powered electrically active implant inside the fat tissue.

± 200 µV/K, $\rho_{el} = 10$ µΩ m). It is enclosed by a polymer housing with low thermal conductivity ($\kappa_{th} = 0,25$ W/m/K). A leg cross-section of 275×275 µm^2 results in maximum power delivery, as demonstrated in [22].

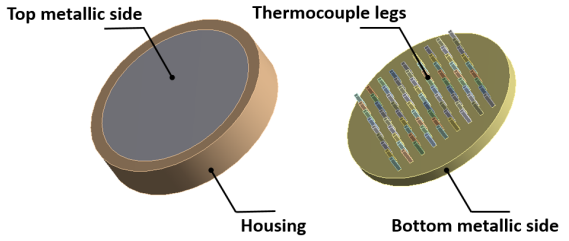

Figure 2: TEG model with cylindrical housing (left) and thermocouple legs array inside (right).

TEG employs the Seebeck effect to transform thermal into electrical energy. The voltage generated is given by:

$$V_{out} = n \cdot \Delta T(\alpha_1 - \alpha_2) \tag{1}$$

where V_{out} is the output voltage, ΔT is the temperature difference accros the thermocouple legs, n is the number of thermocouples and $\alpha_{1,2}$ are the Seebeck coefficients of the thermocouple legs.

A simplified model of human tissue (see Figure 3), which is composed of muscle, fat and skin layer has been chosen for this case study. Thermal material properties of each tissue type are given in Table 1.

Table 1: Thermal material properties of tissue [23].

	muscle	fat	skin
Density (kg/m^3)	1090.4	911	1109
Specific heat capacity (J/kg/K)	3421.2	2348.3	3390.5
Thermal conductivity (W/m/K)	0.4949	0.2115	0.3722

Heat transfer in human tissue is described by the Pennes bioheat equation [24]. This model considers heat

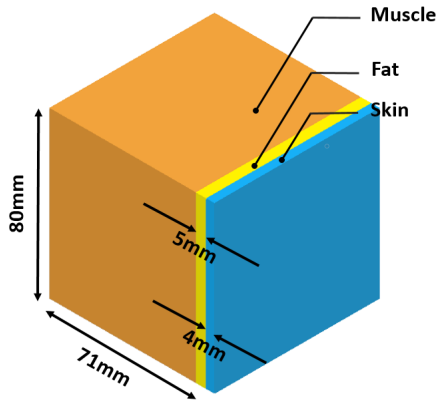

Figure 3: Human tissue model composed of muscle, fat and skin layer (as proposed in [8]).

conduction, metabolic heat generation and temperature-dependent blood perfusion. Currently, we neglect the effect of perfusion and assume a constant metabolic heat generation rate across the muscle tissue. The governing heat-transfer partial differential equation reads:

$$\nabla(\kappa \nabla T) + Q - \rho c \frac{\partial T}{\partial t} = 0 \tag{2}$$

where T is the temperature distribution of interest, ρ, c and κ are the density, specific heat capacity and thermal conductivity properties of each tissue layer specified in Table 1 and $Q = 800$ W/m^3 is a constant metabolic heat generation across the muscle tissue. The body core temperature $T = 37°C$ is accounted for through a Dirichlet boundary condition at the backside of the muscle layer. The heat removal from the skin surface is modeled by convection boundary condition as:

$$q_\perp = h \cdot (T(t) - T_{amb}) \tag{3}$$

where $q_\perp$ is the heat flux normal to the boundary skin surface, T_{amb} is the ambient temperature and h is the film coefficient in W/m^2/K, a parameter dependent on the surface geometry and air velocity. In [25], the following values are given:

$$\begin{cases} h = 3.1 \quad for \quad 0 < v_{air} < 0.2 \\ h = 8.3 {v_{air}}^{0.6} \quad for \quad 0.2 < v_{air} < 4.0 \end{cases} \tag{4}$$

The numerical analysis of the TEG implanted thermal tissue model is carried out by means of FEM. Spatial discretization of the governing PDE (2) with boundary condition (3) leads to a large-scale ODE system of the form:

$$\Sigma_n \begin{cases} E \cdot \dot{T}(t) = A \cdot T(t) + B \cdot u \\ y(t) = C \cdot T(t) \end{cases} \tag{5}$$

where $T \in R^{n\times 1}$ is the vector of unknown temperatures, $E, A \in R^{n\times n}$ are the global heat capacity and heat conductivity matrices respectively, $B \in R^{n\times m}$ is the input matrix and $C \in R^{p\times n}$ is the output matrix with m and p being the number of inputs and user defined outputs respectively. Here the input vector u contains the the heat generation defined in the muscle tissue, whereas the selected outputs are the temperatures at the top and bottom surfaces of the TEG thermocouple legs.

3. Parametric Model Order Reduction

Due to large dimension of (5) ($n = 108292$), the transient simulation is time-consuming. To obtain a compact model, mathematical model order reduction can be used. It is based on an assumption that there exists a low-dimensional subspace $V \in R^{n\times q}$ with $q << n$, that accurately enough captures the dynamics of the state vector $T(t)$:

$$T(t) \approx V \cdot x(t) \tag{6}$$

In the Krylov-subspace based moment matching approach [13], [14], the subspace V is found in such a way that the moments (Taylor coefficients) of the transfer function of (5), defined as:

$$H(s) = C(sE - A)^{-1}B \tag{7}$$

are preserved with respect to the Laplace variable s around some apriori chosen value s_0. For example, the Taylor expansion of (7) around $s_0 = 0$ reads:

$$\begin{aligned} H(s) &= H(0) + \frac{\partial H}{\partial s}(0)\cdot s + \frac{1}{2!}\frac{\partial^2 H}{\partial s^2}(0)\cdot s^2 + \ldots \\ &= \sum_{j=0}^{\infty} \underbrace{-C(A^{-1}E)^j A^{-1}B}_{m_i,\quad i=1,\ldots,q} s^j \end{aligned} \tag{8}$$

The expansion coefficients m_i are called moments of the transfer function. When V is defined as an orthonormal bases of the following Krylov subspace:

$$\begin{aligned} colspan\{V\} &= \mathcal{K}_q\{A^{-1}E, A^{-1}B\} \\ &= \{A^{-1}B, (A^{-1}E)A^{-1}B, \ldots, (A^{-1}E)^q A^{-1}B\} \end{aligned} \tag{9}$$

one obtains a low-dimensional model of order q by projecting (5) onto V as follows:

$$\Sigma_q \begin{cases} \underbrace{V^T E V}_{E_r}\dot{x} = \underbrace{V^T A V}_{A_r}x + \underbrace{V^T B}_{B_r}u \\ y = \underbrace{CV}_{C_r}x \end{cases} \tag{10}$$

The transfer function of (10) is defined as:

$$H_r(s) = C_r(sE_r - A_r)^{-1}B_r \tag{11}$$

and its Taylor expansion around $s_0 = 0$ reads:

$$\begin{aligned} H_r(s) &= H_r(0) + \frac{\partial H_r}{\partial s}(0)\cdot s + \frac{1}{2!}\frac{\partial^2 H_r}{\partial s^2}(0)\cdot s^2 + \ldots \\ &= \sum_{j=0}^{\infty} \underbrace{-C_r(A_r^{-1}E_r)^j A_r^{-1}B_r}_{m_i^{(r)},\quad i=1,\ldots,q} s^j \end{aligned} \tag{12}$$

The property of the Krylov subspace (9) is such that the first q moments m_i and $m_i^{(r)}$ of (8) and (12) are matched and hence, the reduced model is an accurate approximation of the full-scale one. Unfortunately, this approach does not preserve the parameters, which might arise in (5) due to geometry-parametrization or boundary conditions.

For example, in our study of human TEG we seek to investigate the environmental influence upon the temperature difference across the thermocouple legs, by varying the film coefficient and ambient temperature. The parameterized model reads:

$$\Sigma_n \begin{cases} E\cdot\dot{T}(t) = \underbrace{(A_0 + h\cdot A_1)}_{=:A(h)}\cdot T(t) + B\cdot \underbrace{\begin{bmatrix} Q \\ h\cdot T_{amb} \end{bmatrix}}_{=:u} \\ y(t) = C\cdot T(t) \end{cases} \tag{13}$$

The goal of parametric model oder reduction (pMOR) methods is to construct the parameter-independent projection subspace $\tilde{V}$, which can be done by treating the transfer function (7) as a function of two variables (s and h):

$$\tilde{H}(s,h) = C\{sE - (A_0 + h\cdot A_1)\}^{-1}B \tag{14}$$

The Taylor expansion of (14) around, e.g. $(s_0 = 0, h_0 = 0)$ reads:

$$\begin{aligned} \tilde{H}(s,h) = {} & \tilde{H}(0,0) + \frac{\partial\tilde{H}}{\partial s}(0,0)\cdot s + \\ & \frac{\partial\tilde{H}}{\partial h}(0,0)\cdot h + \frac{1}{2!}\frac{\partial^2\tilde{H}}{\partial s^2}(0,0)\cdot s^2 + \\ & \frac{\partial^2\tilde{H}}{\partial s\partial h}(0,0)\cdot s\cdot h + \frac{\partial^2\tilde{H}}{\partial h\partial s}(0,0)\cdot s\cdot h + \\ & \frac{1}{2!}\frac{\partial^2\tilde{H}}{\partial h^2}(0,0)\cdot h^2 + \ldots \end{aligned} \tag{15}$$

In [16], it was proposed to neglect mixed moments and construct the projection subspace V in such a way, to match only the moments with respect to s and h separately. In [26] we demonstrated that this indeed works well if the parameters are not physically correlated, as it is the case for the Laplace variable and the film coefficient. Therefore, two disjoint Krylov subspaces are computed where one parameter is kept constant, while the Krylov subspace is generated for another (variable) parameter and

vice versa; for example, derivatives with respect to s at $s = s_0$ are computed by fixing $h = h_0$. Projection subspaces are generated as:

$$colspan\{V_s\} = \mathcal{K}_{q_1}\{(A(h_0) - s_0E)^{-1}E, (A(h_0) - s_0E)^{-1}B\} \tag{16}$$

$$colspan\{V_h\} = \mathcal{K}_{q_2}\{(A(h_0) - s_0E)^{-1}A_1, (A(h_0) - s_0E)^{-1}B\} \tag{17}$$

Orthonormal bases V_s and V_h are finally merged into a single projection matrix $\tilde{V}$:

$$colspan\{\tilde{V}\} = colspan\{V_s, V_h\} \tag{18}$$

Boundary condition independent ROM now reads:

$$\Sigma_q \begin{cases} \underbrace{\tilde{V}^T E \tilde{V}}_{E_r}\dot{x} = \underbrace{\tilde{V}^T A_0 \tilde{V}}_{A_{0r}}x + h\underbrace{\tilde{V}^T A_1 \tilde{V}}_{A_{1r}}x + \underbrace{\tilde{V}^T B}_{B_r}\cdot \underbrace{\begin{bmatrix} Q \\ h \cdot T_{amb} \end{bmatrix}}_{=:u} \\ y = \underbrace{C\tilde{V}}_{C_r}x \end{cases} \tag{19}$$

where $E_r, A_{0r}, A_{1r} \in R^{(q_1+q_2)\times(q_1+q_2)}$, $B_r \in R^{(q_1+q_2)\times m}$ and $C_r \in R^{p\times(q_1+q_2)}$. The transfer function of (19) is defined as:

$$\tilde{H}_r(s,h) = C_r\{sE_r - (A_{0r} + h \cdot A_{1r})\}^{-1}B_r \tag{20}$$

and its Taylor expansion around e. g. $(s_0 = 0, h_0 = 0)$ reads:

$$\begin{aligned} \tilde{H}_r(s,h) = &\tilde{H}_r(0,0) + \frac{\partial \tilde{H}_r}{\partial s}(0,0)\cdot s + \\ &\frac{\partial \tilde{H}_r}{\partial h}(0,0)\cdot h + \frac{1}{2!}\frac{\partial^2 \tilde{H}_r}{\partial s^2}(0,0)\cdot s^2 + \\ &\frac{\partial^2 \tilde{H}_r}{\partial s \partial h}(0,0)\cdot s \cdot h + \frac{\partial^2 \tilde{H}_r}{\partial h \partial s}(0,0)\cdot s \cdot h + \\ &\frac{1}{2!}\frac{\partial^2 \tilde{H}_r}{\partial h^2}(0,0)\cdot h^2 + \ldots \end{aligned} \tag{21}$$

Property of the Krylov subspaces (16) and (17) is such that only the chosen numbers q_1 respectively q_2 of encirceled terms in (15) and (21) are matched. The allover dimension of the reduced system (19) is $q_1 + q_2$.

As to the difference from [26], we are here interested in studying the static temperature distribution, that is temperature difference across the thermocouple legs, for different environmental conditions (different h and T_{amb}), we might neglect the time-dependent terms in models (13) and (19) and set $\tilde{V} = V_h$, while previously setting $s_0 = 0$ in (17). This speeds up the time for the construction of reduced order model, as only a single Krylov subspace (17) needs to be constructed.

4. Simulation Results

In this section, the accuracy of the parameterized reduced order model is verified and a setup for the system-level simulation is presented.

We performed stationary analyses of the full model (13) with film coefficient and ambient temperature as parameters in range defined in Table 2, that is for 36 different parameter combinations.

Table 2: Parameter values of film coefficient and ambient temperature

v_{air} (m/s)	<0.2	0.8	1.4	2.6	3.2	3.8
h (W/m^2/K)	3.1	7.26	10.157	14.725	16.679	18.491
T_{amb} (K)	10	14	18	22	26	30

Different environmental conditions affect the temperature distribution inside the tissue and hence, the temperature difference across the TEG. Figure 4 illustrates this impact.

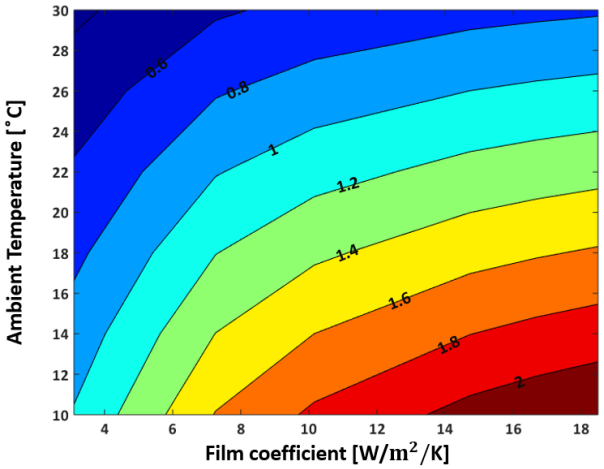

Figure 4: Temperature difference in [°C] across the TEG as a function of film coefficient and ambient temperature.

As expected, a combination of high film coefficient of $h = 18.49$ W/m^2/K and a low ambient temperature of $T_{amb} = 10$ °C leads to a maximum temperature difference of 2.18 °C. A corresponding output voltage amounts to $V_{out} = 70.63$ mV for this model. Furthermore, we evaluated the parametrized reduced order model (19) within stationary simulations over the same parameter space. The stationary full-size model with dimension $n = 108,292$ was reduced to dimension $q_2 = 4$, that is only four moments around $h_0 = 10$ have been matched. Figure 5 compares the temperature difference across the TEG, as obtained from the full and the reduced models. Figure 6 illustrates the relative error.

The maximum relative error between the full and the reduced model amounts to 0.003% which indicates that the parametrized reduced order model is an excellent

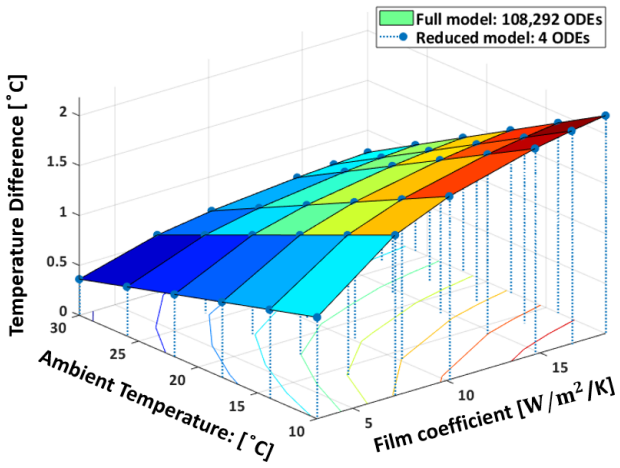

Figure 5: Comparison of temperature differences across the TEG as obtained from the full and the reduced models.

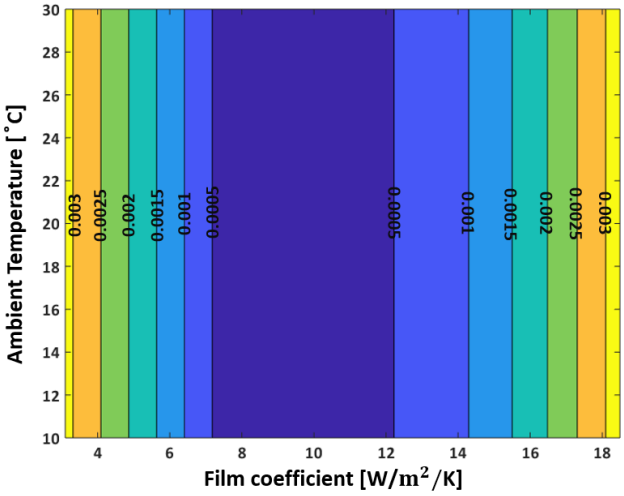

Figure 6: Relative error in temperature difference across the TEG between the full and the reduced models as a function of film coefficient and ambient temperature.

substitute for the original large-scale model in parametric simulation. Note that, the minimum error occurs around $h = 10$ W/m^2/K, as $h_0 = 10$ was chosen for computing the Krylov subspace (17), that is the four moments around $h_0 = 10$ were matched for the full and reduced models. Furthermore, as T_{amb} is a part of the model input in (13) and (19) and hence, is not taken into account during the pMOR process, it does not impact the accuracy of the reduced model (see Figure 6).

Finally, the computational time for a single stationary solution of each parametrized full model is 9.1 s, which makes 327.6 s for parameter study within a 6×6 parameter space. To create a parametrized reduced order model via constructing a single Krylov subspace (17) requires 8.142 s. However, when a parameterized reduced model is available, its integration only takes 665 μs, which makes 0.0024 s for the complete parameter space. Hence, through the pMOR we have achived a speed up of several orders of magnitude. The CPU times are displayed in Table 3.

Table 3: CPU times for running the pMOR and conducting the parameter study on a 6×6 parameter space (on Intel(R) Core(TM) i5-7600 CPU @ 3.5 GHz, 32 GB RAM).

Reduction time (s)	8.142
	Full model (108,292 ODEs)	Reduced model (4 ODEs)
CPU time for 36 static simulations (s)	327.6	0.0024

Furthermore, the small dimension of the parameterized reduced order model enables its co-simulation with electronic circuit. For this purpose it can be imported into a system-level simulator as a state-space model, which provides the temperature difference across the TEG for different environmental conditions (see Figure 7).

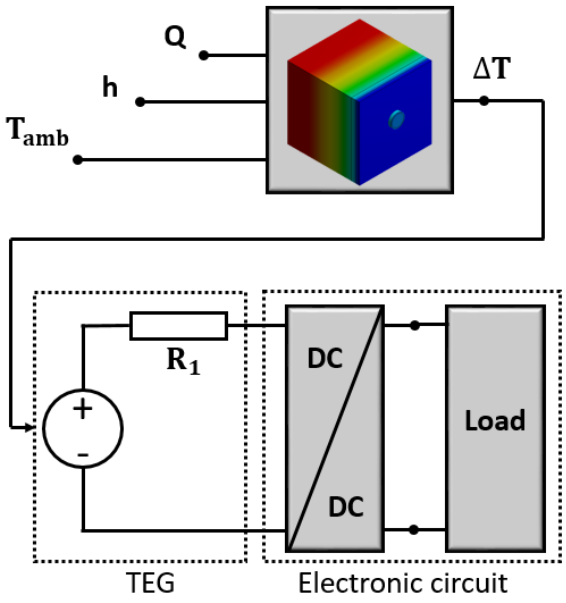

Figure 7: System-level model containing the parametric reduced model and the electronic circuit. R_1 represents the internal resistance of the TEG and the DC/DC converter provides a suitably voltage-level for the application.

5. Summary and Outlook

In this paper, we demonstrated the successful application of parametric model order reduction (pMOR) for generation of a highly accurate and compact thermal model of a human TEG, which can be employed for parametric studies. It allows for efficient investigation of the impact of environmental conditions (e.g. change of film coefficient and ambient temperature) to the temperature distribution across the TEG and can be employed within the system-level simulation as well.

In the future, we aim for a more realistic tissue model, which implements the heat generation by blood perfusion within all tissue layers, as well as radiation and sweating. This requires the development of novel, non-linear pMOR methods. Furthermore, the parametrization of the TEG geometry and the subsequent MOR is in our focus as well.

References

[1] ©Statista 2017. Statistisches bundesamt; oec; ims research.

[2] S. Priya et al. Energy harvesting technologies. Springer, 2009.

[3] C. Y. Tsui et al. Energy harvesting and power delivery for implantable medical devices. *Foundations and Trends®in Electronics Design Automation*, 7:179–246, 2013.

[4] M. A Hannan et al. Energy harvesting for the implantable biomedical devices: issues and challenges. In *BioMedical Engineering OnLine*, 2014.

[5] A. B. Amar et al. Power approaches for implantable medical devices. *Sensors*, 15:28889–28914, 2015.

[6] B. Lu et al. Ultra-flexible piezoelectric devices integrated with heart to harvest the biomechanical energy. *Sci. Rep. 5, 16065*, 2015.

[7] A. Chen. Thermal energy harvesting with thermoelectrics for self-powered sensors: With applications to implantable medical devices, body sensor networks and aging in place. *PHD Thesis, Unversity of California, Berkeley*, 2011.

[8] Y. Yang et al. Suitability of a thermoelectric power generator for implantable medical electronic devices. *in Journal of Physics D: Applied Physics*, 40:5790–5800, 2007.

[9] M. Koplow et al. Thick film thermoelectric energy harvesting systems for biomedical applications. In *Medical Devices and Biosensors, 5th International Summer School and Symposium on*, pages 322–325, 2008.

[10] A. Cadel et al. Kinetic and thermal energy harvesters for implantable medical devices and biomedical autonomous sensors. *Meas. Sci. Technol.*, 25,012003, 2014.

[11] K. Parsons. Human thermal environments. Taylor&Francis, 2003.

[12] A. C. Antoulas. Approximation of large-scale dynamical systems. In *Society for Industrial and Applied Mathematics*, 2005.

[13] R. W. Freund. Krylov-subspace methods for reduced-order modeling in circuit simulation. *Journal of Computational and Applied Mathematics*, 123:395–421, 2000.

[14] Z. J. Bai. Krylov subspace techniques for reduced-order modeling of large-scale dynamical systems. *Applied Numerical Mathematics*, 43:9–44, 2002.

[15] T. Bechtold et al. *System-level Modeling of MEMS*. Wiley-VCH Verlag GmbH & Co. KGaA, 2013.

[16] P. Gunupudi et al. Multi-dimensional model reduction of vlsi interconnects. In *Proceedings of IEEE Custom Integrated Circuits Conference*, pages 499–502, 2000.

[17] D. S. Weile et al. Analysis of frequency selective surfaces using two-parameter generalized rational krylov model-order reduction. *IEEE Transactions on Antennas and Propagation*, 49:1539–1549, 2001.

[18] P. K. Gunupudi et al. Passive parameterized time-domain macromodels for high-speed transmission-line networks. *IEEE Transcations on Microwave Theory and Techniques*, 51:2347–2354, 2003.

[19] L. Daniel et al. A multiparameter moment-matching model-reduction approach for generating geometrically parameterized interconnect performance models. *IEEE Transactions on Computer-Aided Design of Integrated Circuits and Systems*, 23:678–693, 2004.

[20] L. H. Feng. Parameter independent model order reduction. *Mathematics and Computers in Simulation*, 68:221–234, 2005.

[21] E. B. Rudyni et al. Parameter preserving model reduction for mems system-level simulation and design. In *5th MathMod, Proceedings*, pages 3–901608. ISBN, October 2006.

[22] O. Jadhav et al. Design of a thermoelectric generator for electrical active implants. In *MikroSystemTechnik Congress*, pages 1–4, 2017.

[23] IT'IS Foundation. https://www.itis.ethz.ch/virtual-population/tissue-properties/database/heat-capacity/.

[24] H. H. Pennes. Analysis of tissue and arterial blood temperatures in the resting human forearm. *in Journal of applied physiology*, 1:93–122, 1948.

[25] D. Mitchell. Convective heat loss from animals and man. In *in J.L.Monteith and L.E.Mount (Eds), Heat Loss from Animals and Man*. London:Butterworths, 1974.

[26] T. Bechtold et al. Efficient extraction of thin-film thermal parameters from numerical models via parametric model order reduction. *J. Micromech. Microeng.*, 20:045030, 2010.